ACS OMEGA

http://pubs.acs.org/journal/acsodf

Article

Surface-Mounted Dipolar Molecular Rotors Driven by External Electric Field, As Revealed by Torque Analyses

Yan-Ling Zhao,[#] Wanxing Lin,[#] Kulpavee Jitapunkul, Rundong Zhao,[*] Rui-Qin Zhang,[*] and Michel A. Van Hove[*]

Cite This: *ACS Omega* 2022, 7, 35159−35169

Read Online

ACCESS | Metrics & More | Article Recommendations | Supporting Information

ABSTRACT: Driven by a high-speed rotating electric field (*E*-field), molecular motors with polar groups may perform a unidirectional, repetitive, and GHz frequency rotation and thus offer potential applications as nanostirrers. To drive the unidirectional rotation of molecular motors, it is crucial to consider factors of internal charge flow, thermal noise, molecular flexibility, and so forth before selecting an appropriate frequency of a rotating *E*-field. Herein, we studied two surface-mounted dipolar rotors of a "caltrop-like" molecule and a "sandwich" molecule by using quantum−mechanical computations in combination with torque analyses. We find that the rotational trend as indicated by the magnitude and the direction of torque vectors can sensitively change with the lag angle (α) between the dipolar arm and the *E*-field. The atomic charges timely flow within the molecule as the *E*-field rotates, so the lag angle α must be kept in particular intervals to maintain the rotor's unidirectional rotation. The thermal effect can substantially slow down the rotation of the dipolar rotor in the *E*-field. The flexible dipolar arm shows a more rigid geometry in the *E*-field with higher rotation speed. Our work would be useful for designing *E*-driven molecular rotors and for guiding their practical applications in future.

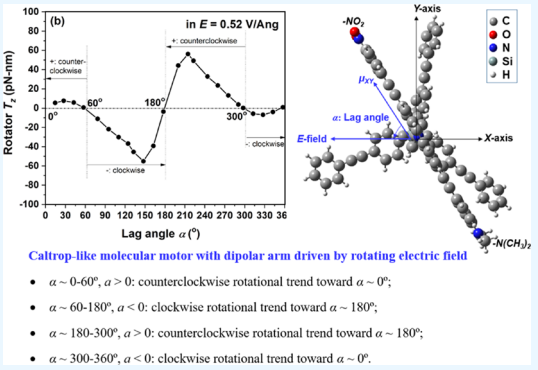

1. INTRODUCTION

Molecular motors play a key role in the innovation of mechanical energy control technology in the microdomain.[1−6] Generally speaking, a molecular motor is expected to transform input energy into rotational motion so as to reach the goal of driving other mechanical components at the nanoscale. In the past decades, various input energy sources have been investigated. These include light,[7−13] chemical reactions,[14−17] scanning tunneling microscopy (STM) tips (electrically driven),[18−23] electric currents,[24,25] and electric fields (*E*-field).[26−32] The present study will focus on molecular motors with rotating *E*-field as the input.

Molecules with permanent dipoles that can rotate in response to an external *E*-field have the potential to act as rotational molecular motors.[33−39] An essential requirement is that such motors should rotate relatively freely on the supporting substrates. At the same time, as a source of input energy, a rotating *E*-field should force the polar rotor to rotate despite the random thermal motion, the friction resistance within the molecule and against the support or solution, and against the mechanical load as it performs work,[1] by external control of the field's magnitude and direction. Zheng et al.[34] fabricated and characterized two surface-mounted altitudinal rotors, one nonpolar and the other dipolar, on a gold surface and have provided evidence that at room temperature, the flipping of the rotator in a fraction of dipolar rotors is subject to a small enough barrier to occur spontaneously and can be controllable by the *E*-field of an STM tip, with a typical run observed (rotation frequency of 90 GHz at room temperature in the *E*-field strength of 3×10^9 V/m, i.e., 0.3 V/Ang). Zhang et al.[39] reported that a two-dimensional array of dipolar molecular rotors (with polar groups of −CN and −O−n−Bu) made from porphyrin-based doubledecker complexes can undergo simultaneous rotational switching when applying an *E*-field from the tip of an STM. Simpson et al.[40] reported how single dipolar molecules (with polar groups of $-NO_2$ and $-N(CH_3)_2$) can be oriented with maximum precision using the *E*-field of an STM. Such *E*-driven molecular motors offer exciting opportunities in the fields of nanoelectronics and nanofluidics.[41,42] On this basis, we model two representative molecules to exhibit their rotational behavior under an *E*-field. We will point out to what extent this behavior is affected by their quantum nature and by thermal effects, compared with

Received: July 1, 2022
Accepted: July 18, 2022
Published: September 20, 2022

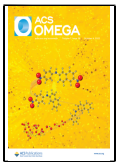

https://doi.org/10.1021/acsomega.2c04128
ACS Omega 2022, 7, 35159−35169

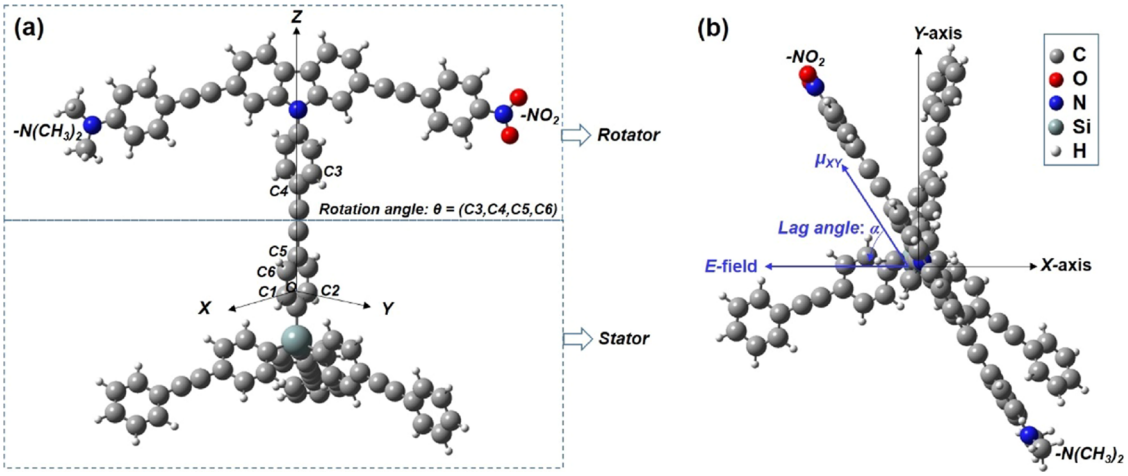

Figure 1. (a) Side view and (b) top view of an *E*-driven "caltrop-like" rotor, with the labeling of key atoms and definition of two dihedral angles θ and α and of the coordinate system. For calculating torques, the midpoint between the carbon atoms C1 and C2 is defined as the origin *O*; the direction from *O* to C1 is set as the *X*-axis and that from *O* to C5 as the *Z*-axis; the perpendicular direction to the *XZ* plane is set as the *Y*-axis. The molecule can be mounted on a surface (in the *XY* plane) with an *E*-field added along the $-X$ direction, viz. perpendicular to the rotation axis (*Z*-axis) of the molecule. Because the stator part is frozen in the calculations, the calculation model does not include the surface. To simulate the rotation of the dipolar arm around the *Z*-axis, the rotation angle θ (C3, C4, C5, and C6) is manually fixed at 0, 15, 30,..., 345° (θ = 60° in Figure 1) when performing constrained geometry optimizations. To study the change of the rotational trend with the angle between the dipolar arm and the *E*-field, the lag angle α is defined as the counterclockwise angle from the $-NO_2$ arm to *E* ($-X$ direction). As the intrinsic dipole moment projected onto the *XY* plane (μ_{XY}) is always basically parallel to the $-NO_2$ arm during rotation, the lag angle α is calculated by using the intrinsic dipole moments projected onto the *X*-axis (μ_X) and *Y*-axis (μ_Y).

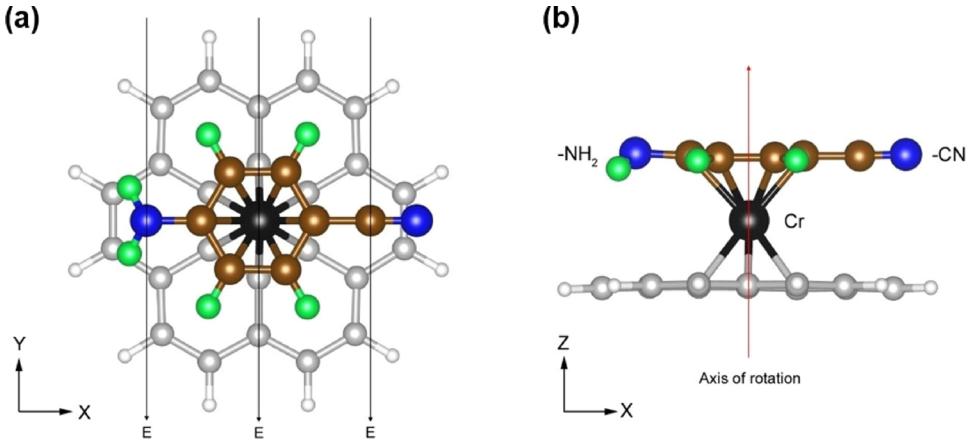

Figure 2. (a) Top view and (b) side view of a "sandwich" rotor, where a dipolar p-cyanoaniline (C in brown, N in blue, and H in green) is as the rotator, an axial Cr atom (in black) as a pivot, and a finite graphene sheet (C in light gray and H in silver) as the stator. The *E*-field is set parallel to the graphene surface, in the $-Y$ direction, viz. perpendicular to the rotation axis (*Z*-axis) of the rotor.

classical rigid dipoles. In particular, we will illustrate the role of molecular flexibility and internal charge flow under the *E*-field. We will also examine how different *E*-field profiles can be used to cause continuous unidirectional rotation.

First, we choose to study a promising molecule that was experimentally synthesized by Jian and Tour[33] (see Figure 1), although its rotation was not examined in the experiment. If the *E*-driven molecular motor rotates in the GHz frequency range,[30] for example, it may cause a directional flow of the surrounding gas or liquid, which is the prototype of a nanoscale pump.[26] This molecule consists of a rotating dipolar arm attached to a static "caltrop-like" structure that is characterized by four tetrahedrally oriented diphenylacetylenes (Ph−C≡C−Ph) that are linked together through a Si atom. Our computational modeling aims to help guide its applications by simulating the *E*-driven intramolecular rotation while revealing the working mechanism at the atomic level. The two ends of the rotating arm are the dipolar groups $-NO_2$ (electron-withdrawing) and $-N(CH_3)_2$ (electron-donating), which endow the arm with a strong permanent dipole moment μ and thus interact with the *E*-field to drive the intramolecular rotation. The stator can be held static as attached to a surface by functionalizing the "free" ends of its three legs (such as with −SH groups) so that this "caltrop-like" molecule becomes an azimuthal rotor on a surface.

Our second, artificial "sandwich" molecule has a much smaller and simpler structure (see Figure 2) and is designed to study more extensively the choice of different types of *E*-fields. Here, we choose a benzene ring as the skeleton, in which two opposite hydrogen atoms are replaced by the groups $-NH_2$ (electron-donating) and −CN (electron-withdrawing). It then becomes a dipolar rotor. We attach it to a finite graphene-like

https://doi.org/10.1021/acsomega.2c04128
ACS Omega 2022, 7, 35159−35169

sheet through a pivot − a chromium (Cr) atom. The Cr atom obeys the effective atomic number rule and connects the two π systems, forming a stable sandwich structure. We then use this model to study this "sandwich" rotor's rotation torque under a fixed *E*-field along the $-Y$ direction and discuss the possibilities of driving a unidirectional rotation by alternatively switching the direction of *E*-fields.

To examine the mechanical behavior of a dipolar molecule in an external *E*-field, we utilize our torque approach[43] as a tool to analyze the intramolecular rotation based on snapshots collected from the rotational trajectory. This torque approach has been validated in previous studies, where we successfully studied the rotational behaviors of a light-driven molecular rotor[43−45] and interlocking molecular gears on surfaces.[46−49] Moreover, torque analysis is widely used in the study of biophysics, such as the transcription of RNA polymerase,[50,51] F1-ATPase,[52] bacterial flagellar motor,[53,54] and kinesin.[55] In this study, we extend the torque approach to the investigation of *E*-field-driven molecular motors. The atomic coordinates and interatomic forces are calculated at the quantum mechanical level, from which the torque vectors acting on each atom of the rotator can easily be obtained. Individual atomic torques clearly reveal which atoms are promoting or hindering the rotation. The total torque profiles (the cumulated atomic torques) help us determine under what conditions the rotation is unidirectional. By presenting results consistent with experiment, the torque approach has been verified to be a reliable method for studying general molecular motors.

In practical applications, thermal noise will inevitably affect the operation of *E*-field-driven molecular machines.[26] To understand how the stochastic rotation (resulting from thermal effects) modifies the molecular response to the *E*-field, we will also track the rotation within the caltrop-like molecule at room temperature by quantum mechanical-based molecular dynamics (MD) simulations. The difference of the response time (i.e., the time for the rotator to relax from an initial nonequilibrium configuration to a stable configuration, which is theoretically parallel to the *E*-field) obtained by static calculation and MD simulation can reflect the relative impact of thermal effects. Additionally, the MD simulation trajectories under an *E*-field can intuitively observe the molecular flexibility change during rotation, which will be also discussed in this work.

With this work, we expect to set up a systematic scheme for the theoretical study of *E*-field-driven molecular motors and therefore help guide the design of more promising molecular motors in future.

2. METHODOLOGY AND COMPUTATIONAL APPROACH

To study the rotation behavior of the large "caltrop-like" rotor (see Figure 1), we carry out quantum mechanical calculations by using the density functional theory (DFT) method (with the ωB97XD[56] functional available in the Gaussian 09[57] package) and the self-consistent charge density functional tight-binding with a dispersion term (DFTB-D) method.[58−62] The detailed calculation procedure will be the following:

(1) Constrained geometric optimizations of 24 configurations are performed at the level of ωB97XD/6-31G* and DFTB-D, with the stator atoms frozen, the dihedral angle θ between the rotator and the stator manually fixed as 0, 15, 30,..., or 345°, and the other rotator atoms fully relaxed. The rotation angle θ (C3, C4, C5, and C6) is determined by atoms C3 and C4 in the rotator as well as atoms C5 and C6 in the stator, where C4 and C5 are located on the rotation *Z*-axis (see Figure 1a). In this way, we can know the profiles of intrinsic dipole moment and potential energies for the "caltrop-like" rotor during 360° rotation without an *E*-field.

(2) To study how the *E*-field timely affects the rotational trend, that is, the coupling between the rotor and the *E*-field, we mark the relative position between the rotor arm and the *E*-field for those structures collected from the rotational trajectory. The lag angle α is thus proposed with the meaning of the counterclockwise angle from the $-NO_2$ arm to the $-X$ direction (the *E*-field direction in Gaussian calculations in this work); see Figure 1b. As the intrinsic dipole moment projected onto the *XY* plane (μ_{XY}) is basically parallel to the $-NO_2$ arm during rotation, the lag angles can be calculated according to the μ_X and μ_Y vectors.

(3) Based on the configurations obtained from the rotational trajectory, we turn on the *E*-field along the $-X$ direction and perform DFT single-point calculations to determine its effect on the charge redistribution, dipoles, and energetics as a function of the lag angle α. We use our recently developed torque analysis method to carefully analyze its rotational trend variation in *E*-field by depicting the torque profiles of the total rotator, functional groups, and key atoms. The torque along the *Z*-axis (T_Z) contributed from any atom, group, or subunit in the molecule can be evaluated by the atomic torque summation formula $\vec{T}_z = \sum_{i=1}^{n} (\vec{r}_i \times F_i\rightarrow)$, where atomic $F_i\rightarrow$ can be obtained from the DFT calculations and $r_i\rightarrow$ is the position of atom *i* relative to the origin *O*. Notably, because of computer code constraints, the *E*-field is permanently oriented along the fixed $-X$ direction (i.e., C1-*O* direction) while the molecular rotator rotates. This does not affect the study of the rotor in a high-speed rotating *E*-field as these configurations are just for samplings with various lag angles.

(4) To investigate the thermal effect and the flexibility of the dipolar arm in an external *E*-field, we next carry out DFTB-D/MD simulations to determine the response times of the dipolar arm at the room temperature in the *E*-field and track the rotation snapshots of the rotator during the MD simulations. The canonical ensemble (NVT) is adopted with the Andersen thermostat at 300 K. The time step is set as 1 fs for the integration of the equations of motion by the Verlet velocity algorithm. The difference of the response time obtained by static DFTB-D calculation and DFTB-D/MD simulation can qualitatively reflect the relative impact of thermal effects. Notably, the substrate and solvents are not included and modeled in the DFTB/MD simulations.

For the small "sandwich" rotor (see Figure 2), to investigate its rotation behavior under the *E*-field, we perform DFT calculations using the Vienna Ab initio Simulation Package (VASP)[63] based on the projector augmented wave[64] with a cut-off energy of 400 eV. The PBE functional[65] is considered sufficient for a qualitative study. Spin polarization and van der Waals interactions[66] are also included. Similarly, constrained geometry optimizations are performed to obtain its potential

https://doi.org/10.1021/acsomega.2c04128
ACS Omega 2022, 7, 35159−35169

energy profile and then the torque profiles in an *E*-field using our torque approach.

Both molecules have their electric dipole oriented approximately perpendicular to their rotation axis, which in turn is oriented approximately perpendicular to a supporting surface. With an *E*-field parallel to this surface, the dipoles therefore tend to point parallel to the *E*-field. In a simple classical picture of a rigid electric dipole $\vec{\mu}$ in a uniform time-independent *E*-field $\boldsymbol{E}\rightarrow$, the energy *U* of the dipole varies as $U = \boldsymbol{E}\rightarrow \cdot \vec{\mu} = E\mu\cdot\cos\alpha$, where α is the lag angle: thus, *U* can vary between $+E\mu$ for an antiparallel alignment and $-E\mu$ for a parallel alignment.

3. RESULTS AND DISCUSSION

3.1. Profiles of Energetic and Dipole Moment without an External *E*-Field. A small rotation barrier and high dipole moment (μ) inherent in the molecule are commonly the two main factors that ensure that a molecular rotor can spin in an applied *E*-field. To understand these two factors in the "caltrop-like" rotor, we perform constrained optimization of its potential energy surface (PES) without an external *E*-field. As shown in Figure 3, the DFTB-D method

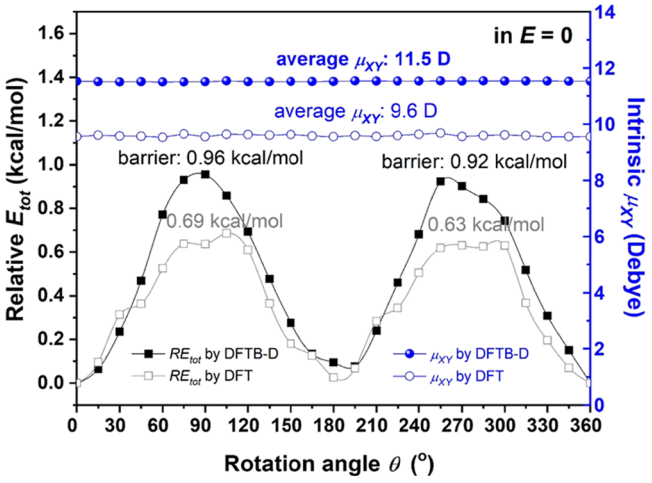

Figure 3. Profiles of the potential energy surface, given as relative energy referred to the energy minimum, and the intrinsic dipole moment values in the *XY* plane (μ_{XY}) for the "caltrop-like" rotor's 360° rotation without an *E*-field.

predicts two small rotation barriers (V_b) of 0.96 and 0.92 kcal/mol during the 360° rotation; the average dipole moment value in the *XY* plane (μ_{XY}) is as high as ~11.5 D and essentially independent of the rotation angle θ. The shallow barriers and steady dipole moment values make this "caltrop-like" molecule a good candidate for an *E*-driven molecular motor, even though it is not inherently unidirectional because of a practically symmetrical PES profile. DFT (ωB97XD/6-31G*) calculations give consistent results with two lower V_b values of 0.69 and 0.63 kcal/mol and a stable average μ_{XY} value as high as ~9.6 D, validating the accuracy of the DFTB-D results. The PES profiles by flexible scanning do not look smooth because of the fact that the small energy barriers of the rotor in $E = 0$ result in the high sensitivity of the PES outline to the energy fluctuations caused by structural changes.

Four additional characteristics can be found in the above results: (1) Because there are two arms and three legs in this "caltrop-like" molecule, the PES profile should present six barriers during the 360° rotation. However, only two energy barriers are found in Figure 3, which reflects that the three legs have negligible impact on the rotator because of the long axial distance (~1.3 nm) between the arms of the rotator and the legs of the stator. This PES profile is actually similar to that of a Ph−C≡C−Ph molecule, as calculated using the same theoretical parameters, where two V_b of ~0.53 kcal/mol appear when the two phenyl rings are perpendicular to each other. (2) We find that this constrained optimization has no significant effect on the tangential forces that govern the rotation of the dipolar arm; the changed radial forces can be neglected with this relatively rigid dipolar arm. (3) The dipole moment μ always points to the rotator arm during the 360° rotation (see Movie S1). The isosurface distribution of the electrostatic potential (see Figure S1) demonstrates that the μ direction results predominantly from the significant negative and positive charges on the $-NO_2$ and $-N(CH_3)_2$ groups, respectively. Therefore, it is reasonable to use the $-NO_2$ arm direction as a reference to study the relationship between the rotation behavior and the lag angle α. (4) We note that the thermal energy *kT* at room temperature is about 25 meV (~0.58 kcal/mol), which is not far from the molecular rotation barrier. This suggests that the thermal vibrations may play a non-negligible role in the rotation of this "caltrop-like" molecule. This issue will be examined further below through DFTB-D/MD simulations.

3.2. Energetic, Dipole Moment, Charge Distribution, and Rotational Trend Affected by the External *E*-Field. We next consider the effect of the *E*-field on the rotational trend of the dipolar arm. Twenty-four configurations are selected from the abovementioned optimizations (with $E = 0$), and then, the field of $E = 0.52$ V/Ang (0.01 a.u.) is applied along the $-X$ direction. The *E*-field strength of 0.52 V/Ang is comparable to the studies of Michl's group.[28,34] Figure S2 shows these 24 configurations with the lag angle α specified. On this basis, single-point energy calculations in *E*-field by DFT (ωB97XD/6-31G*) are performed to study the change of PES, dipole moment, and charge population and analyze the rotational trend through torque profiles; see Figure 4. We have verified at selected lag angles that results from constrained geometry optimizations are close to those of single-point calculations; see Table S1.

Figure 4a shows the profiles of the single-point PES E_{tot} and dipole strength in the *E*-field. The instantaneous dipole moment keeps changing as the arm rotates in the *E*-field. Very conspicuous is the strong variation of the electric dipole and its much-enhanced value compared to the case with $E = 0$ (maximum 108.5 vs 11.5 D). Even larger is the resulting change in the barrier height, with rotation V_b of 87 kcal/mol for $E = 0.52$ V/Ang, compared to less than 1 kcal/mol for $E = 0$.

The intrinsic reason behind the strong variation of instantaneous dipole moments is the charge redistribution on the $-NO_2$ and $-N(CH_3)_2$ groups; see Figure 4b. Specific charge data are listed in Tables S2 and S3. Here, the charge distribution within the rotator has been re-optimized without re-optimizing the atomic coordinates. At $\alpha = 180°$, the $-N(CH_3)_2$ and $-NO_2$ groups are, respectively, forced to carry more positive and negative charges (than they are in $E = 0$) so as to cause the largest instantaneous dipole moment. At $\alpha = 0°$, the charges on $-N(CH_3)_2$ and $-NO_2$ groups reflect the strongest counteracting effect between the permanent dipole moment and the *E*-field, resulting in a much-reduced dipole

https://doi.org/10.1021/acsomega.2c04128
ACS Omega 2022, 7, 35159−35169

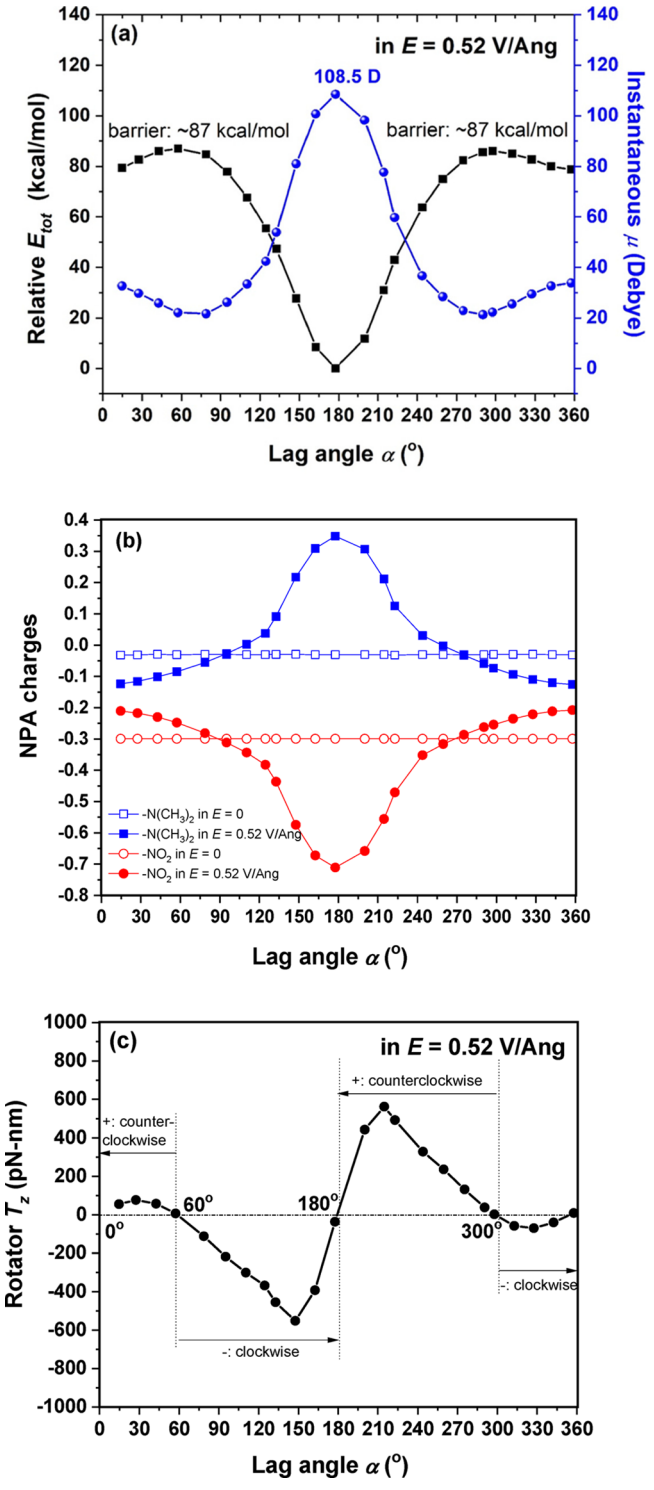

Figure 4. (a) Single-point PES E_{tot} and instantaneous dipole moment μ in E = 0.52 V/Ang of the configurations shown in Figure S2. (b) Total natural partial atomic (NPA) charges of the $-NO_2$ and $-N(CH_3)_2$ groups in E = 0.52 V/Ang vs E = 0 V/Ang, based on natural bond orbital analysis. (c) Total torque projected onto the Z-axis (T_z) of the rotator in E = 0.52 V/Ang.

moment, even reversing the net charge sign on the $-N(CH_3)_2$ group. This also contributes to the anomalous (additional) local energy minimum seen in Figure 4a near α = 0°. Therefore, we can conclude that the lag angle α can sensitively characterize the rotational behavior, which is influenced by the rapidly changing interaction between the molecular dipole moment and the E-field.

Figure 4c confirms that the rotator torque T_z is essentially proportional to the derivative of the total energy relative to the lag angle (just as in classical mechanics where the force is proportional to the derivative of the potential). The slope of the PES reflects the driving force, as is seen when comparing the PES (Figure 4a) and the torque profile (Figure 4c). The presence of a second energy minimum near α = 0° causes a total of four instances of zero values for T_z at α = ~0, 60, 180, and 300°. The most extreme torque values occur at ~150 and 210° (not 90 and 270° as in the simple cos α model), with two minor extrema ~30 and 330°. It implies that the angular velocity ω of the dipolar arm rotation in the E-field constantly changes as the angular acceleration a is directly proportional to the torque T_z ($T_z = Ia$, minimal changes of the moment of inertia I of the molecule can be neglected). Assuming positive and negative torques correspond to counterclockwise and clockwise acceleration, the rotational behavior is therefore determined to be in four α ranges, as noted in Figure 4c:

- $\alpha \sim 0-60°$, $a > 0$: counterclockwise rotational trend toward $\alpha \sim 0°$;
- $\alpha \sim 60-180°$, $a < 0$: clockwise rotational trend toward $\alpha \sim 180°$;
- $\alpha \sim 180-300°$, $a > 0$: counterclockwise rotational trend toward $\alpha \sim 180°$;
- $\alpha \sim 300-360°$, $a < 0$: clockwise rotational trend toward $\alpha \sim 0°$.

When driven by a rotating E-field parallel to a surface, surface-mounted azimuthal molecular motors can exhibit synchronous, asynchronous, and random rotation modes, which are related to the strength and frequency of the E-field.[3] As the factors impeding unidirectional rotation become more prominent, a synchronous (i.e., periodic) rotation with the rotating E-field may become an asynchronous (i.e., nonperiodic) rotation. The response time will be lengthened due to a reduction of the rotation velocity, and the molecular motor may even become unusable. Therefore, α should be kept in particular intervals to maintain the rotor's unidirectional rotation.

3.3. Atomic Torque and Group Torque Analyses for Unidirectional Rotation. The total torque on a molecule or molecular fragment is the vector sum of all individual atomic torques. However, individual atomic torques may have different vector signs from the total torque, namely, they can be positive or negative due to different lag angles of atoms relative to the E-field. The main contribution to atomic T_z is found to come from the $-N(CH_3)_2$ and $-NO_2$ groups, as highlighted in Figure 5a. The magnitude of the atomic torque on each atom in E = 0.52 V/Ang varies over time with the lag angles; even the torque sign can change, which will hinder or promote the unidirectional rotation. For example, the atomic T_z of atom N_a in $-N(CH_3)_2$ dramatically varies with the lag angle in the E-field. It promotes the unidirectional rotation for α = 60–150° and 300–360° when the atomic T_z sign is then consistent with the total T_z shown in Figure 4c, while hindering the rotation for α = 0–60 and 150–300° as the atomic T_z sign is then opposite to the total T_z. This can also be ascribed to the significant charge alteration of this atom N_a affected by the E-field, as indicated by the NPA charges in Figure 5b. Moreover, it is found that the torques of atom pairs bonding with each other often have opposite signs, for

https://doi.org/10.1021/acsomega.2c04128
ACS Omega 2022, 7, 35159–35169

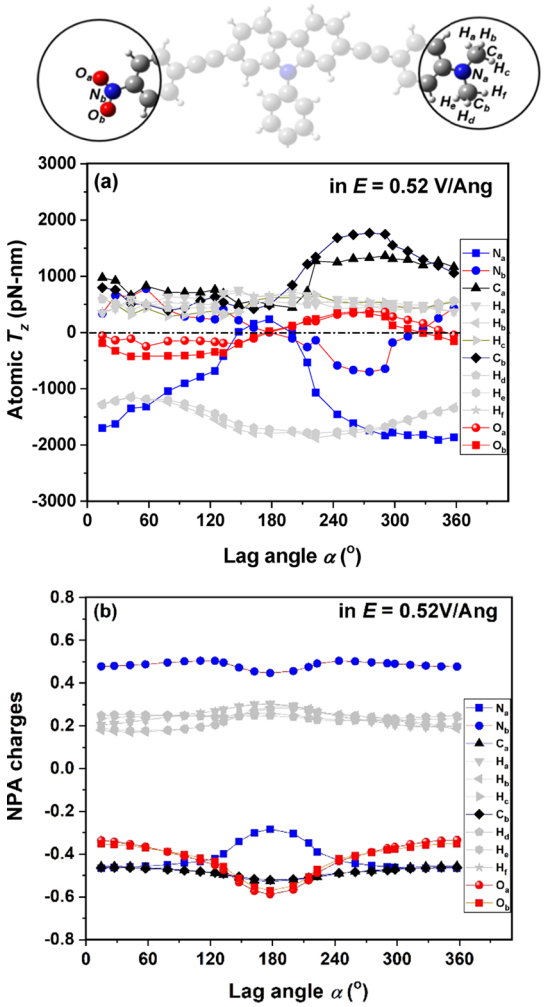

Figure 5. Profiles of (a) atomic torques and (b) NPA charges of individual atoms in the $-NO_2$ and $-N(CH_3)_2$ groups in E = 0.52 V/Ang, as a function of the lag angle α. The top panel shows the atom labels of two polar groups.

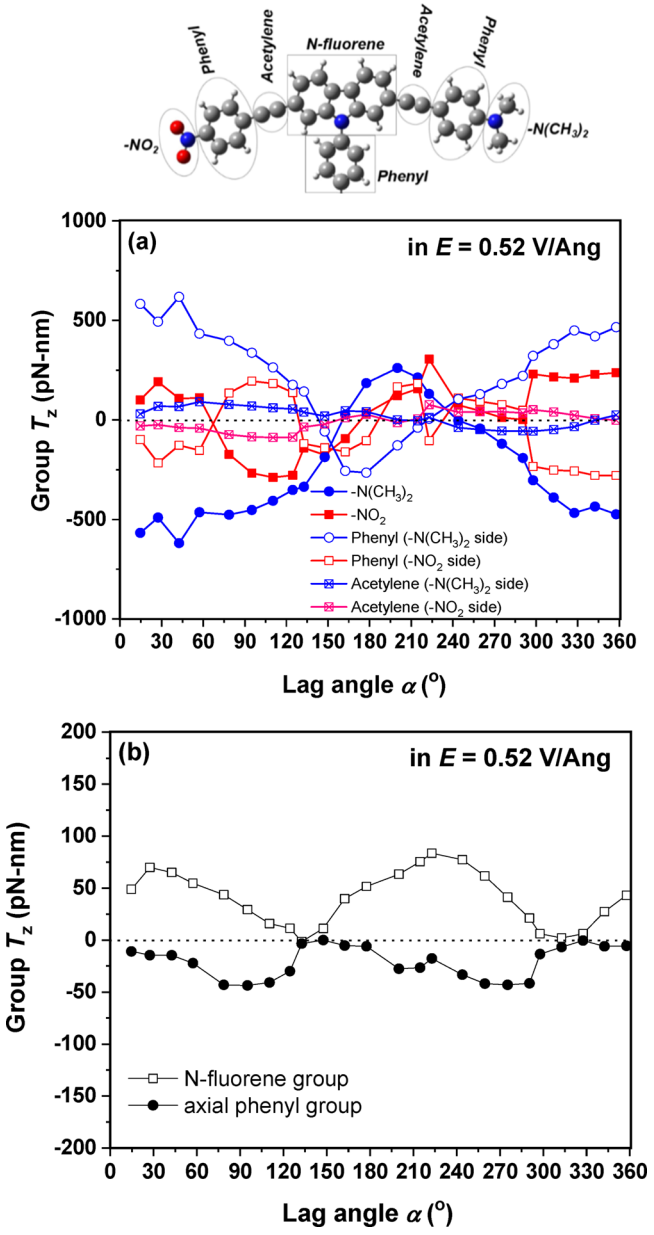

Figure 6. Torques contributed by different chemical groups in E = 0.52 V/Ang as a function of the lag angle α. (a) Chemical groups in the two arms. (b) Chemical groups on the axis of the rotator, viz. the N-fluorene group and the phenyl group. Top panel shows the names of the chemical groups in the rotator.

example, the torque of the N atom in $-NO_2$ and the torque of the two O atoms in $-NO_2$, the torque of the N atom in $-N(CH_3)_2$ and the torque of the two C atoms in $-N(CH_3)_2$, and so forth. Most of the atomic torques are ineffective after their mutual counteraction. The remaining net torques may be small but can still force the dipolar arm to rotate with the E-field. Therefore, in the practical applications of E-driven molecular motors, the changing atomic T_z with the lag angle will mutually interplay in a synergistic or counteracting manner.

Also, torque analysis for the entire groups of atoms sometimes may provide helpful information for understanding large molecular rotors. The present molecular rotator comprises several subunits including the $-N(CH_3)_2$ and $-NO_2$ groups, the phenyl and acetylene groups on the two arms, the fluorene and phenyl groups on the rotation axis, and so forth. It is thus inferred that the forces among chemical groups may generate group torques with different signs. As shown in Figure 6a, in the ranges of α = 0−60 and 300−360°, the almost mirror-symmetrical T_z distributions above and below zero reflect the significant offsetting effect between the two acetylene groups in different arms and between the $-N(CH_3)_2/-NO_2$ group and the phenyl group in the same arm. Only when the coupling between the molecule and the E-field is strong enough (e.g. for $\alpha \approx [90°, 170°]$ and $\alpha \approx [190°, 270°]$) can the cooperation among these functional groups be obvious. There also exists a partial counteracting effect between the fluorene and phenyl groups on the axis; see Figure 6b. Referring to the total T_z in Figure 4c, it is thus found that the remaining T_z can genuinely lead to the unidirectional rotation of the molecular motor after excluding the counteracting parts.

3.4. Influence of the Thermal Effect. Static calculations are insufficient to ascertain the unidirectionality of molecular motors in their practical applications. The friction and thermal effects in real situations may also play an important role in affecting the rotation. The fluctuating force can be governed by the vibrations in the support, by the viscosity of the solution

https://doi.org/10.1021/acsomega.2c04128
ACS Omega 2022, 7, 35159−35169

and by temperature (so-called thermal noise). Work can be produced for a surface-mounted rotor placed anywhere as long as there are temperature fluctuations, although the work may just cause random clockwise and counterclockwise rotations, which is not very useful for mechanical applications.[67]

To understand how the stochastic rotation resulting from thermal effects modifies the molecular response to the *E*-field, we will also track the rotation within the "caltrop-like" molecule at room temperature by DFTB-D/MD simulations. For that purpose, we qualitatively evaluate the response time of the rotor, defined here as the time needed for the molecule to rotate from rest in a nonequilibrium orientation until becoming parallel to the *E*-field. The difference of the response time obtained by static DFTB-D calculation and DFTB-D/MD simulation can then qualitatively reflect the relative impact of thermal effects on the unidirectional rotation. As a preliminary study of the *E*-field-driven molecular motor, the MD simulation in this work is done in the absence of solvents.

In a proper molecular motor, the rotating frequency should be high enough to reach the GHz level[30] (i.e., period time ∼ 1000 ps, average angular velocity $\omega \sim 0.36°$/ps) in order to work effectively in the microscopic field. A prerequisite is that the molecule's response speed should be much faster than the *E*-field's rotation speed so as to synchronously follow the rotating *E*-field. This means that the dipolar arm actually settles from a nonequilibrated state into an equilibrated state in a very short time; otherwise, asynchronous or random rotation may happen because of torque repositioning (including changes in the value and direction), as evidenced by Figure 4c.

Figure 7 reveals the response time with thermal effect considered, for the "caltrop-like" rotor from nonequilibrated to

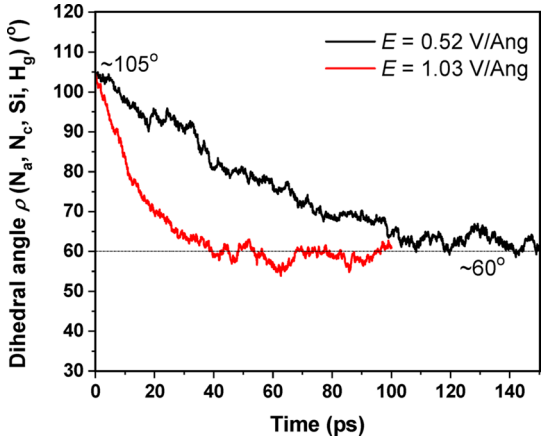

Figure 7. Evolution of the dihedral angle ρ in the DFTB-D/MD simulation for the "caltrop-like" molecule in E = 0.52 V/Ang and 1.03 V/Ang. Here, ρ is defined by the four atoms N_a, N_c, Si, and H_g, as shown in Figure S3.

equilibrated states by DFTB-D/MD simulations at room temperature in E = 0.52 and 1.03 V/Ang. The "caltrop-like" configuration with $\alpha = 135°$ (Counterclockwise angle from the $-NO_2$ arm to the *E*-field is 135°) is selected as the study case; see Figure S3. For convenience, the dihedral angle ρ (N_a, N_c, Si, H_g) is marked to track its time evolution so as to reflect the response time. In E = 0.52 V/Ang, the dynamic process from an initial nonequilibrated state with $\alpha = 135°$ to a final equilibrated state (parallel to *E*) with $\alpha = 180°$ is completed in ∼100 ps, accompanied with the change in ρ from ∼105 to ∼60°; see Movie S2. ρ is stabilized at ∼60° from 100 to 150 ps. Therefore, the average angular velocity of this "caltrop-like" molecule can be estimated to be ∼0.45°/ps ($\Delta\alpha/t$ = 45°/100 ps), which meets the GHz level requirement in molecular motor applications.

To find the average angular velocity dominated by only the potential energy, the static calculation on the nonequilibrated configuration (see Figure S3a,b) under the same condition of E = 0.52 V/Ang and $\alpha \sim 135°$ was carried out using the DFTB-D method. According to Newton's second Law, the response time of the dipolar arm with the clockwise rotational trend toward $\alpha \sim 180°$ can be concluded as follows:

$$T_z = Ia = I\frac{\omega}{t} = I\frac{\Delta\alpha}{t^2} \Rightarrow t = \sqrt{\Delta\alpha I/T_z},\ \omega = \frac{\Delta\alpha}{t}$$

Here, the value of total T_z can be obtained using our torque approach; I is the moment of inertia of the rotator ($I = 4.6 \times 10^{-43}$ kg m^2 for the "caltrop-like" rotor); a is the rotator's angular acceleration; $\Delta\alpha = 45°$ (from 135 to 180°); t is the response time of the dipolar arm, which is thus roughly estimated to be 1.70 ps; and the average angular velocity ω is accordingly ∼26.5°/ps. The response time results (see Table 1) shed light on the rotor's performance, revealing that the

Table 1. Comparison of the Influence on the Response Time in an *E*-Field[a]

E-field intensity, *E* (V/Ang)	response time, *t* (ps) by static DFTB-D calculations	response time, *t* (ps) by DFTB-D/MD simulations
0.52	1.70	100
1.03	0.82	40

[a]The influence from static potential energy (middle column) and the influence from the thermal effect (right column). The MD response time listed in Table 1 was estimated from a single trajectory for a qualitative comparison.

thermal effect dramatically reduces the rotation velocity by approximately two orders of magnitude. However, if we apply an *E*-field with higher intensity (say, E = 1.03 V/Ang), the response time from the static calculation and the MD simulation (see Movie S3) can be 0.82 and ∼40 ps, respectively. This shows that the ratio between the internal potential energy and thermal effect on the response time can be substantially tuned by enhancing the intensity of the *E*-field.

3.5. Flexibility Change of the Large Molecular Rotor under an External *E*-Field. The flexibility of large molecules has always been a non-negligible feature of molecular machines.[46] Taking the typical "caltrop-like" molecule of this study as an example, we report the distortion effect caused by the external *E*-field.

To understand the geometric flexibility changes of the "caltrop-like" molecule during the unidirectional rotation driven by an *E*-field, the bending and twisting of the dipolar arm were analyzed by using representative snapshots selected from the DFTB-D/MD simulation trajectories at E = 0.52 and 1.03 V/Ang (see Movies S2 and S3). In E = 0.52 V/Ang, the dynamic simulation of the clockwise intramolecular rotation starts from the configuration shown in Figure 8a and stops at the configuration shown in Figure 8i, so does that for E = 1.03 V/Ang (see Figure S4). We still use the dihedral angle ρ (N_a, N_c, Si, H_g) to track the arm orientation in the whole MD simulation. The *E*-field direction is marked with a blue arrow

https://doi.org/10.1021/acsomega.2c04128
ACS Omega 2022, 7, 35159−35169

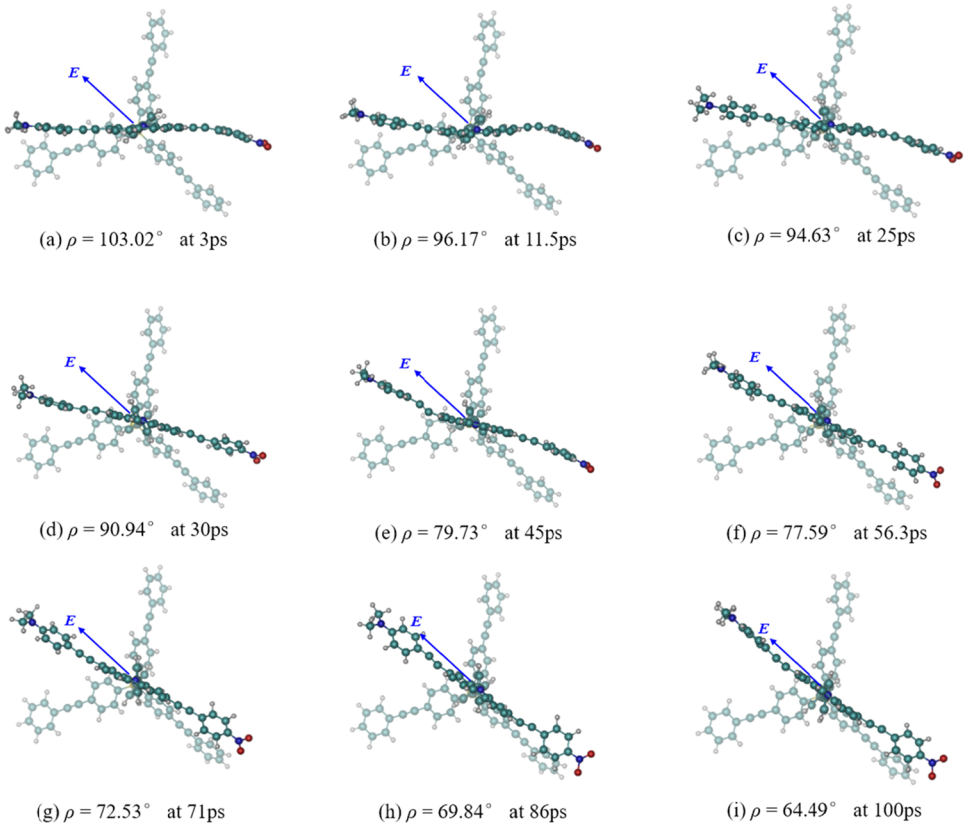

Figure 8. Top views of the selected snapshots for (a) ρ = 103.02° at 3 ps, (b) ρ = 96.17° at 11.5 ps, (c) ρ = 94.63° at 25 ps, (d) ρ = 90.94° at 30 ps, (e) ρ = 79.73° at 45 ps, (f) ρ = 77.59° at 56.3 ps, (g) ρ = 72.53° at 71 ps, (h) ρ = 69.84° at 86 ps, and (i) ρ = 64.49° at 100 ps, from the DFTB-D/MD simulation trajectory for the unidirectional rotation of the "caltrop-like" molecular motor driven by E = 0.52 V/Ang.

for tracking the clockwise rotation during the dynamic simulation.

We see in Figure 8 that the dipolar arm is S-shaped because of the strong pull of the E-field on the $-NO_2$ and $-N(CH_3)_2$ groups. Such a deformation is much more obvious in the first few snapshots because the arm has significant lag angles with E. However, when the arm becomes nearly parallel to E, the E-field tends to straighten it out. In addition, we see rotations around the length of the molecular arm itself, as can be observed in Figure 8, from the top view of the $-NO_2$ and $-N(CH_3)_2$ groups and also from the phenyl rings in the arm. These are caused by the intermolecular interactions between the rotator and the stator. When the E-field intensity increases from 0.52 to 1.03 V/Ang, the S-shaped feature of the dipolar arm becomes much less obvious (see Figure S4). This could be due to the quicker response of the dipolar arm to the stronger E-field, which leads to less deformation in the middle steps of the MD process. It is thus conjectured that the dipolar arm will show a more rigid geometry in the practical application of an E-field with a higher rotation speed.

3.6. Unidirectional Rotation of a Small Rigid Rotor Driven by a High-Speed Rotating *E*-Field. To enhance the understanding of the effect of an external E-field on the unidirectional rotation of a small rigid rotor, we adopt a dipolar "sandwich" rotor (see Figure 2) as an ideal model. Figure 9a shows the PES outline of the "sandwich" rotor in an E-field of 0.52 V/Ang, as the molecule rotates through 360°. If the molecules were a rigid dipole, this profile would have the shape of $U = \boldsymbol{E}\rightarrow\cdot\vec{\mu} = -E\mu\cdot\cos(\theta\text{-}90°)$: the minimum would occur at 90°, while the maximum would occur at 270°. The actual profile of Figure 9a basically follows the rigid-dipole cosine profile. The total torque and individual torque on atom groups projected along the rotation axis are shown in Figure 9b, which clearly indicate that the N atom of the −CN group is the largest contributor to the total torque acting on the "sandwich" molecule and greatly promotes its unidirectional rotation, while the other atoms basically counteract each other during the rotor's rotation.

The PES deviations from the cosine profile, which particularly strike near 270°, reflect the significant charge redistribution within the molecule, as evidenced by the special charge populations on two dipolar groups at the rotation angles of 265, 270, and 275°; see Table 2. More importantly, we can also see in Figure 9b the small perturbation of the sign of the total torque at the rotation angles near 270°. It can be correlated with the off-axis positioning of the atoms H_1 and H_2 of the NH_2 group and their resulting differential charge fluctuations under rotation.

4. CONCLUSIONS

In this work, we have computationally studied the rotational characteristics of two dipolar rotors of a "caltrop-like" molecule and a "sandwich" molecule in an E-field. The combination of quantum calculations with the torque analysis method is presented to be a useful approach to study the unidirectional rotation of such molecules. The driving force for the rotor's unidirectional rotation can be quantified into the torque vector acting on the rotator projected on the rotation axis (T_z), which is revealed to sensitively vary with the angle between the dipolar arm and the E-field because of the atomic charge

https://doi.org/10.1021/acsomega.2c04128
ACS Omega 2022, 7, 35159−35169

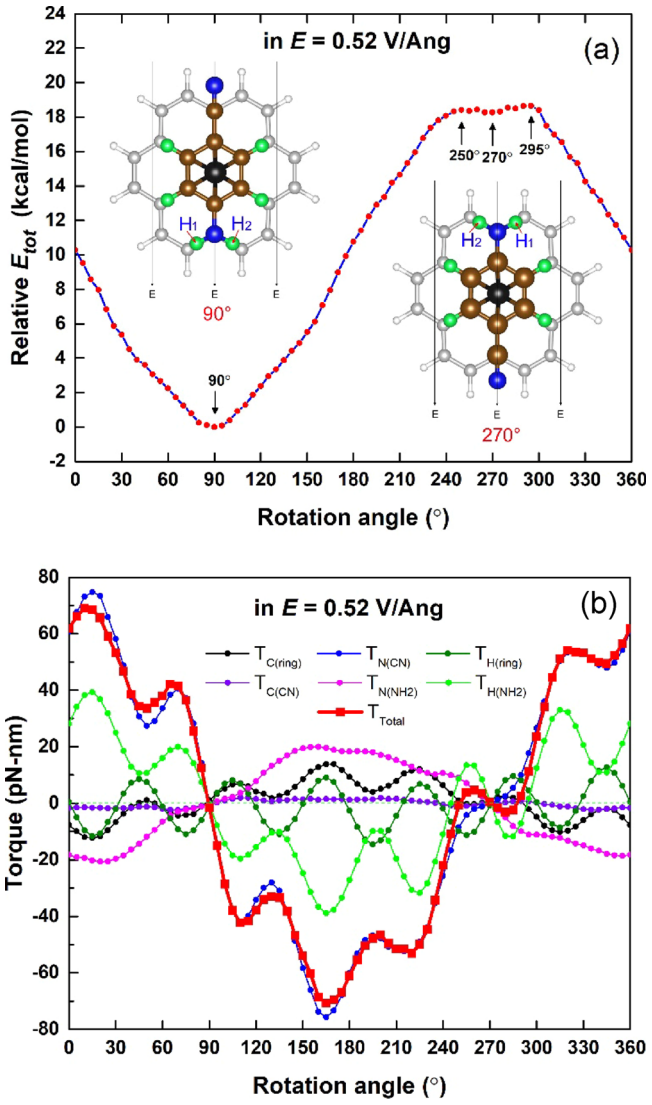

Figure 9. Profiles of the (a) potential energy surface, given as relative energy referred to the energy minimum and (b) total T_z and atomic T_z projected onto the rotation axis of the "sandwich" rotor in an *E*-field of 0.52 V/Ang along the $-Y$ direction. In this case, the rotation angle has the same meaning to the lag angle α. The inset molecular structures demonstrate the configurations at 90 and 270°. For simplicity, we study the profiles of total energies and torques as a function of the rotation angle between the rotator and the stator. The two H atoms of the $-NH_2$ group are indexed as H_1 and H_2. For more details on the rotor's structure, please refer to Figure 2 caption.

redistribution under the influence of the external *E*-field. Torque analysis at each rotation step demonstrates that most torques counteract each other among functional groups while only the remaining net torque leads to collective cooperation within the molecule and promotes unidirectional rotation. To maintain a unidirectional and synchronous rotation, a high-speed rotating *E*-field with appropriate strength is suggested.

The *E*-field-driven molecular rotors in this work are studied in the absence of solvents. Toward the practical applications of *E*-field-driven rotors as a nanostirrer in a fluid, further progress can be made by modeling the rotor in an explicit solvent environment under the *E*-field to clarify how much the solvents/ions shield the *E*-field and how the *E*-field affects the orientations of solvents/ions and noncovalent interactions with the rotor molecule.

■ ASSOCIATED CONTENT

Supporting Information

The Supporting Information is available free of charge at https://pubs.acs.org/doi/10.1021/acsomega.2c04128.

Side view of the "caltrop-like" molecule in all orientations (AVI)

Top view of the "caltrop-like" molecule in all orientations (AVI)

Side-view animations for the MD simulations from the initial nonequilibrated state (α = 135°) to the final equilibrated state (α = 180°) in an electric field of strength *E* = 0.52 V/Ang (the *E*-field direction is shown in Figure S3b), for the "caltrop-like" molecule (AVI)

Top-view animations for the MD simulations from the initial nonequilibrated state (α = 135°) to the final equilibrated state (α = 180°) in an electric field of strength *E* = 0.52 V/Ang (the *E*-field direction is shown in Figure S3b), for the "caltrop-like" molecule (AVI)

Side view animations similar to Movie S2 but with a stronger electric field: E = 1.03 V/Ang (AVI)

Top view animations similar to Movie S2 but with a stronger electric field: E = 1.03 V/Ang (AVI)

Color-coded electrostatic potential distribution on van der Waals surfaces for the "caltrop-like" molecule as calculated by ωB97XD/6-31G*; top views of the 24 molecular motor configurations adopted for the calculations in *E* = 0.52 V/Å; side view and top view of the *E*-field-driven molecular motor with the lag angle α = 135° before MD simulations and the top view of the molecular motor with α = ∼180° in *E* = 0.52 V/Ang after MD simulations; top views of the selected snapshots from the DFTB-D/MD simulation trajectory for the unidirectional rotation of the "caltrop-like" molecular motor driven by *E* = 1.03 V/Å; one table for comparing the differences in dipole moment (μ) and relative total energy (RE_{tot}) between constrained geometry optimizations and single-point calculations in *E* = 0.52 V/Ang; two tables of natural population atomic charges on the $-N(CH_3)_2$ and $-NO_2$ groups in *E* = 0 and 0.52 V/Ang, for the "caltrop-like" molecule (PDF)

Table 2. Atomic Net Charges of the Dipolar Groups in the "Sandwich" Molecule at Particular Rotation Angles[a]

atoms	0° (free)	0°	85°	90°	95°	250°	265°	270°	275°	290°
C(−CN)	0.88	0.81	0.72	0.70	0.72	0.78	0.69	0.65	0.68	0.77
N(−CN)	−1.13	−1.10	−1.10	−1.11	−1.10	−1.02	−0.93	−0.94	−0.92	−1.03
$N(-NH_2)$	−1.19	−1.18	−1.21	−1.24	−1.21	−1.22	−1.26	−1.27	−1.26	−1.22
$H_1(-NH_2)$	0.44	0.44	0.47	0.47	0.46	−0.02	0.02	0.43	0.44	0.44
$H_2(-NH_2)$	0.44	0.46	0.46	0.47	0.47	0.44	0.44	0.44	0.03	0.03

[a]The second column indicates the charges in a free *E*-field, and others indicate the charges in an *E*-field of 0.52 V/Ang (Unit: |*e*|).

https://doi.org/10.1021/acsomega.2c04128
ACS Omega 2022, 7, 35159−35169

AUTHOR INFORMATION

Corresponding Authors

Rundong Zhao − *School of Physics, Beihang University, Beijing 100191, China; Shenzhen JL Computational Science and Applied Research Institute, Shenzhen 518129, China;* orcid.org/0000-0002-5690-1209; Email: rdzhao@buaa.edu.cn

Rui-Qin Zhang − *Department of Physics, City University of Hong Kong, Hong Kong SAR 999077, China; Shenzhen JL Computational Science and Applied Research Institute, Shenzhen 518129, China;* orcid.org/0000-0001-6897-4010; Email: aprqz@cityu.edu.hk

Michel A. Van Hove − *Institute of Computational and Theoretical Studies & Department of Physics, Hong Kong Baptist University, Hong Kong SAR 999077, China;* Email: vanhove@associate.hkbu.edu.hk

Authors

Yan-Ling Zhao − *Department of Physics, City University of Hong Kong, Hong Kong SAR 999077, China; Shenzhen Research Institute, City University of Hong Kong, Shenzhen 518057, China;* orcid.org/0000-0001-5840-9149

Wanxing Lin − *Department of Physics, City University of Hong Kong, Hong Kong SAR 999077, China*

Kulpavee Jitapunkul − *Department of Physics, City University of Hong Kong, Hong Kong SAR 999077, China*

Complete contact information is available at: https://pubs.acs.org/10.1021/acsomega.2c04128

Author Contributions

#Equal contributions: Y.L.Z. and W.L.

Notes

The authors declare no competing financial interest.

ACKNOWLEDGMENTS

This work was financially supported by the Collaborative Research Fund of the Research Grants Council of Hong Kong (C2014-15G), the National Natural Science Foundation of China (21703190, 12104028), and also the Shenzhen Natural Science Foundation (JCYJ20190813164801693). We acknowledge the Beijing Computational Science Research Center, the National Supercomputer Centers in Guangzhou and Shenzhen, and the High-Performance Cluster Computing Centre in Hong Kong Baptist University for providing computational resources.

REFERENCES

(1) Kottas, G. S.; Clarke, L. I.; Horinek, D.; Michl, J. Artificial molecular rotors. *Chem. Rev.* **2005**, *105*, 1281−1376.

(2) Browne, W. R.; Feringa, B. L. Making molecular machines work. *Nat. Nanotechnol.* **2006**, *1*, 25−35.

(3) Vacek, J.; Michl, J. Artificial surface-mounted molecular rotors: molecular dynamics simulations. *Adv. Funct. Mater.* **2007**, *17*, 730−739.

(4) Michl, J.; Sykes, E. C. H. Molecular rotors and motors: recent advances and future challenges. *ACS Nano* **2009**, *3*, 1042−1048.

(5) Coskun, A.; Banaszak, M.; Astumian, R. D.; Stoddart, J. F.; Grzybowski, B. A. Great expectations: can artificial molecular machines deliver on their promise? *Chem. Soc. Rev.* **2012**, *41*, 19−30.

(6) Dattler, D.; Fuks, G.; Heiser, J.; Moulin, E.; Perrot, A.; Yao, X.; Giuseppone, N. Design of collective motions from synthetic molecular switches, rotors, and motors. *Chem. Rev.* **2020**, *120*, 310−433.

(7) Koumura, N.; Zijlstra, R. W. J.; van Delden, R. A.; Harada, N.; Feringa, B. L. Light-driven monodirectional molecular rotor. *Nature* **1999**, *401*, 152−155.

(8) van Delden, R. A.; ter Wiel, M. K. J.; Pollard, M. M.; Vicario, J.; Koumura, N.; Feringa, B. L. Unidirectional molecular motor on a gold surface. *Nature* **2005**, *437*, 1337−1340.

(9) Balzani, V.; Clemente-León, M.; Credi, A.; Ferrer, B.; Venturi, M.; Flood, A. H.; Stoddart, J. F. Autonomous artificial nanomotor powered by sunlight. *Proc. Natl. Acad. Sci. U. S. A.* **2006**, *103*, 1178−1183.

(10) Morin, J.-F.; Shirai, Y.; Tour, J. M. En route to a motorized nanocar. *Org. Lett.* **2006**, *8*, 1713−1716.

(11) Conyard, J.; Addison, K.; Heisler, I. A.; Cnossen, A.; Browne, W. R.; Feringa, B. L.; Meech, S. R. Ultrafast dynamics in the power stroke of a molecular rotary motor. *Nat. Chem.* **2012**, *4*, 547−551.

(12) Léonard, J.; Schapiro, I.; Briand, J.; Fusi, S.; Paccani, R. R.; Olivucci, M.; Haacke, S. Mechanistic origin of the vibrational coherence accompanying the photoreaction of biomimetic molecular switches. *Chem. − Eur. J.* **2012**, *18*, 15296−15304.

(13) Wezenberg, S. J.; Chen, K.-Y.; Feringa, B. L. Visible-light-driven photoisomerization and increased rotation speed of a molecular motor acting as a ligand in a ruthenium(II) complex. *Angew. Chem., Int. Ed.* **2015**, *54*, 11457−11461.

(14) Badjić, J. D.; Balzani, V.; Credi, A.; Silvi, S.; Stoddart, J. F. A molecular elevator. *Science* **2004**, *303*, 1845−1849.

(15) Fletcher, S. P.; Dumur, F.; Pollard, M. M.; Feringa, B. L. A reversible, unidirectional molecular rotary motor driven by chemical energy. *Science* **2005**, *310*, 80−82.

(16) Ye, T.; Kumar, A. S.; Saha, S.; Takami, T.; Huang, T. J.; Stoddart, J. F.; Weiss, P. S. Changing stations in single bistable rotaxane molecules under electrochemical control. *ACS Nano* **2010**, *4*, 3697−3701.

(17) Yang, C.-H.; Prabhakar, C.; Huang, S.-L.; Lin, Y.-C.; Tan, W. S.; Misra, N. C.; Sun, W.-T.; Yang, J.-S. A redox-gated slow-fast-stop molecular rotor. *Org. Lett.* **2011**, *13*, 5632−5635.

(18) Kudernac, T.; Ruangsupapichat, N.; Parschau, M.; Maciá, B.; Katsonis, N.; Harutyunyan, S. R.; Ernst, K.-H.; Feringa, B. L. Electrically driven directional motion of a four-wheeled molecule on a metal surface. *Nature* **2011**, *479*, 208−211.

(19) Tierney, H. L.; Murphy, C. J.; Jewell, A. D.; Baber, A. E.; Iski, E. V.; Khodaverdian, H. Y.; McGuire, A. F.; Klebanov, N.; Sykes, E. C. H. Experimental demonstration of a single-molecule electric motor. *Nat. Nanotechnol.* **2011**, *6*, 625−629.

(20) Sykes, E. C. H. Electric nanocar equipped with four-wheel drive gets taken for its first spin. *Angew. Chem., Int. Ed.* **2012**, *51*, 4277−4278.

(21) Ernst, K.-H. A turn in the right direction. *Nat. Nanotechnol.* **2013**, *8*, 7−8.

(22) Perera, U. G. E.; Ample, F.; Kersell, H.; Zhang, Y.; Vives, G.; Echeverria, J.; Grisolia, M.; Rapenne, G.; Joachim, C.; Hla, S.-W. Controlled clockwise and anticlockwise rotational switching of a molecular motor. *Nat. Nanotechnol.* **2013**, *8*, 46−51.

(23) Zhang, Y.; Calupitan, J. P.; Rojas, T.; Tumbleson, R.; Erbland, G.; Kammerer, C.; Ajayi, T. M.; Wang, S.; Curtiss, L. A.; Ngo, A. T.; Ulloa, S. E.; Rapenne, G.; Hla, S. W. A chiral molecular propeller designed for unidirectional rotations on a surface. *Nat. Commun.* **2019**, *10*, 3742.

(24) Dundas, D.; McEniry, E. J.; Todorov, T. N. Current-driven atomic waterwheels. *Nat. Nanotechnol.* **2009**, *4*, 99−102.

(25) Král, P.; Seideman, T. Current-induced rotation of helical molecular wires. *J. Chem. Phys.* **2005**, *123*, 184702.

(26) Vacek, J.; Michl, J. Molecular dynamics of a grid-mounted molecular dipolar rotor in a rotating electric field. *Proc. Natl. Acad. Sci. U. S. A.* **2001**, *98*, 5481−5486.

(27) Horinek, D.; Michl, J. Molecular dynamics simulation of an electric field driven dipolar molecular rotor attached to a quartz glass surface. *J. Am. Chem. Soc.* **2003**, *125*, 11900−11910.

(28) Horinek, D.; Michl, J. Surface-mounted altitudinal molecular rotors in alternating electric field: single-molecule parametric sscillator

https://doi.org/10.1021/acsomega.2c04128
ACS Omega 2022, 7, 35159−35169

molecular dynamics. *Proc. Natl. Acad. Sci. U. S. A.* **2005**, *102*, 14175−14180.
(29) Wang, B.; Vuković, L.; Král, P. Nanoscale rotary motors driven by electron tunneling. *Phys. Rev. Lett.* **2008**, *101*, No. 186808.
(30) Prokop, A.; Vacek, J.; Michl, J. Friction in carborane-based molecular rotors driven by gas flow or electric field: classical molecular dynamics. *ACS Nano* **2012**, *6*, 1901−1914.
(31) Neumann, J.; Gottschalk, K. E.; Astumian, R. D. Driving and controlling molecular surface rotors with a terahertz electric field. *ACS Nano* **2012**, *6*, 5242−5248.
(32) Akimov, A. V.; Kolomeisky, A. B. Unidirectional rolling motion of nanocars induced by electric field. *J. Phys. Chem. C* **2012**, *116*, 22595−22601.
(33) Jian, H.; Tour, J. M. En route to surface-bound electric field-driven molecular motors. *J. Org. Chem.* **2003**, *68*, 5091−5103.
(34) Zheng, X.; Mulcahy, M. E.; Horinek, D.; Galeotti, F.; Magnera, T. F.; Michl, J. Dipolar and nonpolar altitudinal molecular rotors mounted on an Au(111) surface. *J. Am. Chem. Soc.* **2004**, *126*, 4540−4542.
(35) Daub, C. D.; Bratko, D.; Ali, T.; Luzar, A. Microscopic dynamics of the orientation of a hydrated nanoparticle in an electric field. *Phys. Rev. Lett.* **2009**, *103*, No. 207801.
(36) Kelly, T. R.; Silva, R. A.; Silva, H. D.; Jasmin, S.; Zhao, Y. A rationally designed prototype of a molecular motor. *J. Am. Chem. Soc.* **2000**, *122*, 6935−6949.
(37) Shao, J.; Zhu, W.; Zhang, X.; Zheng, Y. Molecular rotors with designed polar rotating groups possess mechanics-controllable wide-range rotational speed. *npj Comput. Mater.* **2020**, *6*, 185.
(38) Miyazaki, T.; Shoji, Y.; Ishiwari, F.; Kajitani, T.; Fukushima, T. Design of a molecular memory element with an alternating circular array of dipolar rotors and rotation suppressors. *Chem. Sci.* **2020**, *11*, 8388−8393.
(39) Zhang, Y.; Kersell, H.; Stefak, R.; Echeverria, J.; Iancu, V.; Perera, U. G. E.; Li, Y.; Deshpande, A.; Braun, K.-F.; Joachim, C.; Rapenne, G.; Hla, S.-W. Simultaneous and coordinated rotational switching of all molecular rotors in a network. *Nat. Nanotechnol.* **2016**, *11*, 706−712.
(40) Simpson, G. J.; García-López, V.; Boese, A. D.; Tour, J. M.; Grill, L. How to control single-molecule rotation. *Nat. Commun.* **2019**, *10*, 4631.
(41) Liu, W.; Ren, Y.; Tao, Y.; Li, Y.; Chen, X. Controllable rotating behavior of individual dielectric microrod in a rotating electric field. *Electrophoresis* **2017**, *38*, 1427−1433.
(42) Hossan, M. R.; Dutta, D.; Islam, N.; Dutta, P. Review: electric field driven pumping in microfluidic device. *Electrophoresis* **2018**, *39*, 702−731.
(43) Zhang, R. Q.; Zhao, Y. L.; Qi, F.; Hermann, K.; Van Hove, M. A. Intramolecular torque, an indicator of the internal rotation direction of rotor molecules and similar systems. *Phys. Chem. Chem. Phys.* **2016**, *18*, 29665−29672.
(44) Chen, L.; Qi, F.; Jitapunkul, K.; Zhao, Y. L.; Zhang, R. Q.; Van Hove, M. A. Intramolecular torque study of a molecular rotation stimulated by electron injection and extraction. *J. Phys. Chem. A* **2018**, *122*, 7614−7619.
(45) Hermann, K. E.; Qi, F.; Zhao, R.; Zhang, R. Q.; Van Hove, M. A. Fragment motion in motor molecules: basic concepts and application to intra-molecular rotations. *Phys. Chem. Chem. Phys.* **2018**, *20*, 21487−21497.
(46) Zhao, R.; Qi, F.; Zhang, R. Q.; Van Hove, M. A. How does the flexibility of molecules affect the performance of molecular rotors? *J. Phys. Chem. C* **2018**, *122*, 25067−25074.
(47) Zhao, R.; Qi, F.; Zhao, Y. L.; Hermann, K. E.; Zhang, R. Q.; Van Hove, M. A. Interlocking molecular gear chains built on surfaces. *J. Phys. Chem. Lett.* **2018**, *9*, 2611−2619.
(48) Zhao, R.; Zhao, Y. L.; Qi, F.; Hermann, K. E.; Zhang, R. Q.; Van Hove, M. A. Interlocking mechanism between molecular gears attached to surfaces. *ACS Nano* **2018**, *12*, 3020−3029.
(49) Ahmed, S. B.; Ullah, N.; Zhao, Y. L.; Zhang, R. Q.; Van Hove, M. A. Solvents hinder the interlocking rotation between molecular gears, as revealed by torque calculations. *J. Phys. Chem. C* **2021**, *125*, 17612−17621.
(50) Mazur, A. K. Torque transfer coefficient in DNA under torsional stress. *Phys. Rev. E* **2012**, *86*, No. 011914.
(51) Ma, J.; Tan, C.; Gao, X.; Fulbright, R. M., Jr.; Roberts, J. W.; Wang, M. D. Transcription factor regulation of RNA polymerase's torque generation capacity. *Proc. Natl. Acad. Sci. U. S. A.* **2019**, *116*, 2583−2588.
(52) Chou, Y. C.; Hsiao, Y.-F.; Hwang, G.-J.; To, K. Torque Generation through the random movement of an asymmetric rotor: a potential rotational mechanism of the γ subunit of F_1−ATPase. *Phys. Rev. E* **2016**, *93*, No. 022408.
(53) Zhou, J.; Lloyd, S. A.; Blair, D. F. Electrostatic interactions between rotor and stator in the bacterial flagellar motor. *Proc. Natl. Acad. Sci. U. S. A.* **1998**, *95*, 6436−6441.
(54) Wadhwa, N.; Phillips, R.; Berg, H. C. Torque-dependent remodeling of the bacterial flagellar motor. *Proc. Natl. Acad. Sci. U. S. A.* **2019**, *116*, 11764−11769.
(55) Ramaiya, A.; Roy, B.; Bugiel, M.; Schäffer, E. Kinesin rotates unidirectionally and generates torque while walking on microtubules. *Proc. Natl. Acad. Sci. U. S. A.* **2017**, *114*, 10894−10899.
(56) Chai, J.-D.; Head-Gordon, M. Long-range corrected hybrid density functionals with damped atom-atom dispersion corrections. *Phys. Chem. Chem. Phys.* **2008**, *10*, 6615−6620.
(57) Frisch, M. J.; Trucks, G. W.; Schlegel, H. B.; Scuseria, G. E.; Robb, M. A.; Cheeseman, J. R.; Scalmani, G.; Barone, V.; Mennucci, B.; Petersson, G. A., et al.. *Gaussian 09, Revision D.01*; Gaussian, Inc.: Wallingford, CT, 2009.
(58) Porezag, D.; Frauenheim, T.; Köhler, T.; Seifert, G.; Kaschner, R. Construction of tight-binding-like potentials on the basis of density-functional theory: application to carbon. *Phys. Rev. B* **1995**, *51*, 12947−12957.
(59) Elstner, M.; Porezag, D.; Jungnickel, G.; Elsner, J.; Haugk, M.; Frauenheim, T.; Suhai, S.; Seifert, G. Self-consistent-charge density-functional tight-binding method for simulations of complex materials properties. *Phys. Rev. B* **1998**, *58*, 7260−7268.
(60) Elstner, M.; Frauenheim, T.; Kaxiras, E.; Seifert, G.; Suhai, S. A self-consistent charge density-functional based tight-binding scheme for large biomolecules. *Phys. Stat. Sol. (b)* **2000**, *217*, 357−376.
(61) Frauenheim, T.; Seifert, G.; Elstner, M.; Hajnal, Z.; Jungnickel, G.; Porezag, D.; Suhai, S.; Scholz, R. A self-consistent charge density-functional based tight-binding method for predictive materials simulations in physics, chemistry and biology. *Phys. Stat. Sol. (b)* **2000**, *217*, 41−62.
(62) Aradi, B.; Hourahine, B.; Frauenheim, T. DFTB+, A sparse matrix-based implementation of the DFTB method. *J. Phys. Chem. A* **2007**, *111*, 5678−5684.
(63) Kresse, G.; Furthmüller, J. Efficient iterative schemes for *ab initio* total-energy calculations using a plane-wave basis set. *Phys. Rev. B* **1996**, *54*, 11169−11186.
(64) Kresse, G.; Joubert, D. From ultrasoft pseudopotentials to the projector augmented-wave method. *Phys. Rev. B* **1999**, *59*, 1758−1775.
(65) Perdew, J. P.; Burke, K.; Ernzerhof, M. Generalized gradient approximation made simple. *Phys. Rev. Lett.* **1996**, *77*, 3865−3868.
(66) Grimme, S.; Antony, J.; Ehrlich, S.; Krieg, H. A consistent and accurate *ab initio* parametrization of density functional dispersion correction (DFT-D) for the 94 elements H-Pu. *J. Chem. Phys.* **2010**, *132*, 154104.
(67) Astumian, R. D. Thermodynamics and kinetics of a Brownian motor. *Science* **1997**, *276*, 917−922.

https://doi.org/10.1021/acsomega.2c04128
ACS Omega 2022, 7, 35159−35169